Numerical Assessment of Acoustic Installation Effects Characterizing NASA/LaRC Quiet Flow Facility using Computational AeroAcoustics

S. Redonnet

Numerical Assessment of Acoustic Installation Effects Characterizing NASA/LaRC Quiet Flow Facility using Computational AeroAcoustics

Stéphane Redonnet*
ONERA (French Aerospace Centre), BP 72 - 29 av Division Leclerc, Châtillon, 92322, France

This paper presents a numerical assessment of acoustic installation effects characterizing the NASA Langley Quiet Flow Facility (QFF), an open-jet, anechoic wind tunnel. Several Computational Aeroacoustics (CAA) calculations based on equivalent simplistic sources are conducted, enabling the estimation of the installation effects possibly induced by the QFF environment on the measured acoustic signatures during typical airframe noise experiments. First, the conclusions that had been previously made by the present author in an earlier assessment of QFF installation effects onto the so-called Tandem Cylinder experiments are reproduced. Then, these conclusions are extended to various situations which are more representative of the usual airframe noise tests that are typically conducted in the QFF. In particular, this provides an opportunity to compare the refraction/convection effects of the QFF jet flow to the reflection/diffraction induced by the experimental apparatus. All this further aids in the identification of acoustic installation effects that may be important in the type of testing typically done in the NASA/LARC QFF facility.

Nomenclature

α	=	spreading angle of the facility jet mixing layers
D	=	tandem cylinder diameter
f, f_n	=	frequency, frequency of the nth tone
f'_{prim}	=	frequency of the primary shedding acoustic emission
H	=	half height of QFF test section
λ, λ_n	=	wavelength, wavelength of the nth tone
M, T	=	Mach number and temperature
M_∞, T_∞	=	Mach number and temperature at infinity
M_{core}, T_{core}	=	Mach number and temperature in the core of the facility jet
M_r, T_r	=	Mach number and temperature ratio
PSD	=	Power Spectral Density
P_o	=	atmospheric pressure
RMS	=	Root Mean Square
t	=	time coordinate
T_{prim}	=	primary shedding period
x,y,z	=	Cartesian coordinates

I. Introduction

A few years ago, noise annoyances by aircraft were officially identified as the major obstacle to a sustainable growth of air traffic. Therefore, all stakeholders involved in the development of aircraft systems or components now focus on practical ways to reduce the acoustic signature by their products. On another hand, since acoustics is a complex discipline, they are often bounded to make an intensive use of numerical simulations, which constitutes a powerful R&D tool, when used in complement to experimentation. In particular, a synergy must be established between the computational and the experimental worlds, so that each benefit from the other; indeed, whereas it is mandatory that the various numerical techniques are validated through reliable experiments, it is also highly desirable that the latter testing procedures and environments take direct benefit

* PhD, Research scientist, CFD and Aeroacoustics Department, Onera, Stephane.Redonnet@onera.fr.

from the additional information offered by computational means, which can improve the relevance and the confidence in the experimental measurements acquired.

II. Background and Motivation: Numerical Assessment of Acoustic Installation Effects by QFF onto the Tandem Cylinder Experiments, via CFD-CAA Hybrid Calculations

To better understand some of the generic physical mechanisms associated with the aeroacoustics of aircraft undercarriage systems, a combined experimental and computational campaign[1-3] was carried out at NASA Langley Research Center (LaRC), focusing on both the aerodynamics and the acoustics of a Tandem Cylinder (TC) configuration. The model geometry is defined by two identical cylinders, spatially separated in the streamwise direction of an incoming flow. Such a simplified configuration constitutes an ideal test case for investigating the physics of aerodynamic noise associated with component interaction, as well as validating high-fidelity numerical prediction tools for similar sources of noise in actual aircraft systems (landing gears, etc.). To this end, extensive experimental data had been collected[1,2] and compared to the results of 3D, unsteady compressible CFD (Computational Fluid Dynamics) computations[3] (see top/left of Fig. 2), which had been extrapolated to the far-field with the help of an Integral Method (IM) based on a Ffowcs Williams & Hawkings (FWH) technique[4] (see top/right of Fig. 2, in black dashes).

Despite the favorable comparison between the measured and computed results, a legitimate concern existed about some of the obvious differences occurring between the installed TC configuration that had been tested and the simplified configuration that was computed. In other words, questions arose about the fact that these CFD-FWH hybrid calculations did not incorporate any of the possible installation effects that could have occurred in the experiments. Indeed, accounting for all or part of the facility environment (see Fig. 1) during the initial CFD stage would have been far too expensive, requiring a fine mesh to compute not only the cylinders, but also the side walls supporting and surrounding them. On the other hand, as explained above, the intrinsic limitations of Helmoltz-based integral methods[4-6] limited the FWH stage from correctly accounting for the reflection / diffraction and convection / refraction effects that may have been caused by the QFF apparatus and associated jet flow.

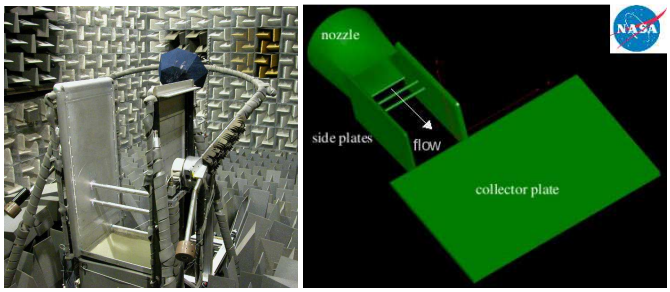

Figure 1. Noise emission of a Tandem Cylinder (TC) installed within NASA/LaRC's Quiet Flow Facility (QFF). *Left side: TC model, with some of the QFF devices (nozzle, mounting side plates). Right side: sketch of the whole installed TC set up, with all the QFF devices (nozzle, mounting side plates, collector plate). Courtesy of NASA.*

Therefore, a dedicated study was conducted, with the objective of numerically investigate the various acoustic installation effects that could have been effectively induced by the experimental set up onto the acoustic data gathered during NASA/LaRC experiments. In particular, it was aimed at investigating not only the effects induced by the solid devices characterizing the experimental apparatus in the anechoic facility, but also by its corresponding (confined and sheared) jet flow. These requirements could be fulfilled by using an advanced acoustic hybrid approach[7] involving a noise propagation stage based on a Computational AeroAcoustics (CAA) technique, so that all acoustic installation effects that were expected to occur due to the QFF environment can be properly accounted for. Indeed, one can here recall that only a CAA method[*] relying on the Euler equations[8-11] or a linearized version thereof can simultaneously account for the reflection/diffraction effects by solid obstacles and the refraction effects by the flow heterogeneities, in contrast to other techniques that can only model the former (such as the Boundary Element Method, BEM), or even neither of them (such as Integral Methods, IM[4-6]). Consequently, several CFD-CAA hybrid calculations of the QFF-installed TC configuration were performed[12], all being based on an identical CFD dataset. The latter was obtained from the isolated TC unsteady CFD computations described above, for which near-field data had been obtained using NASA/LaRC's CFL3D solver. The CFD-CAA weak coupling procedure relied on the so-called *Non Reflective Interface* (NRI) technique[13,14], which allows properly handling acoustic backscattering that is typical of airframe configurations installed within a wind tunnel facility. These CFD-CAA hybrid calculations were performed with a different degree of realism included each time, so as to estimate separately the effect by each component (e.g., mounting side plates, nozzle, collector plate) or feature (e.g., confined jet vs. free co-flow) characterizing the NASA/LaRC QFF facility, so that the impact of each installation effect on the acoustic signature of the TC emission is assessed individually. As an illustration, left bottom of Fig. 2 displays an instantaneous snapshot of the perturbed

[*] whether it is based on high-order finite-difference (FD) schemes operating on multi-block structured grids[4-7], or on the so-called Discontinuous Galerkin Method, which is based on unstructured grids.

pressure field delivered by the CFD-CAA hybrid calculation focusing on the fully installed TC configuration, which included all of the QFF facility main devices, as well as the corresponding confined / sheared jet flow. Such results are compared against the ones obtained for the isolated TC configuration, in terms of far-field noise radiation (see the red and black spectra, in right top of Fig. 2) or near-field acoustic propagation (see the delta effects between the two respective Sound Pressure Level maps, in right bottom of Fig. 2). For more details about this work, the reader is referred to Ref. 12.

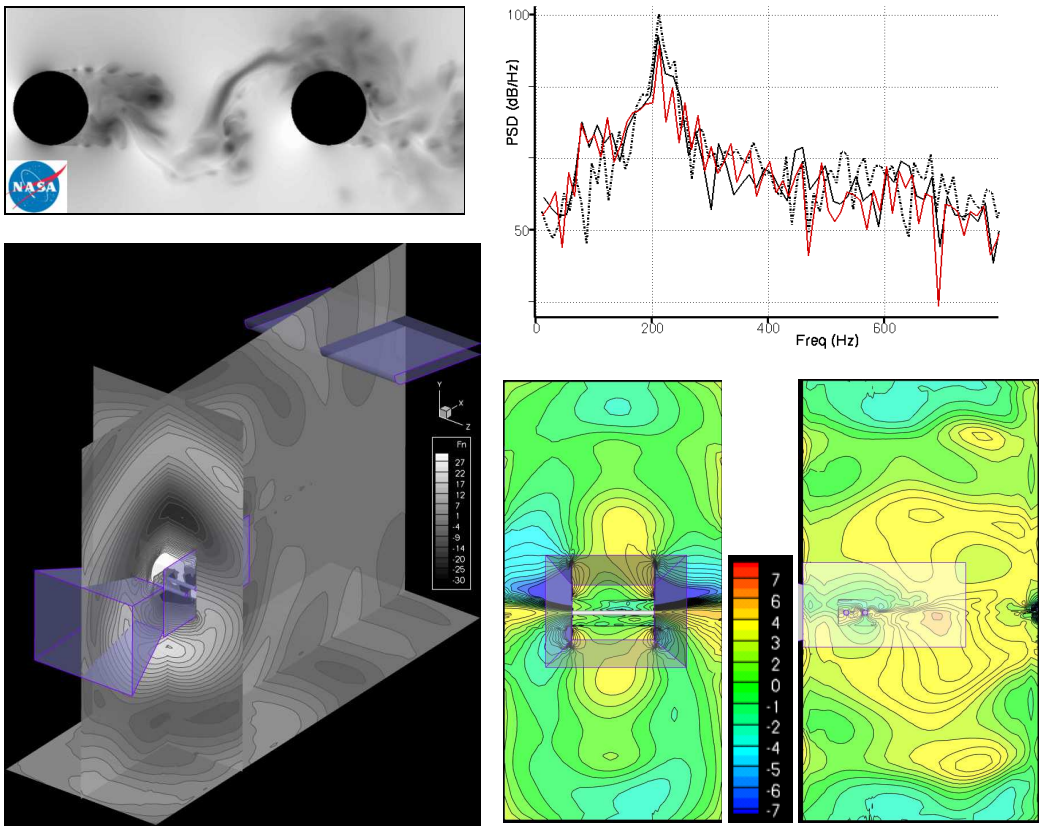

Figure 2. Noise emission of a Tandem Cylinder (TC) installed within NASA/LaRC's QFF anechoic facility, via CFD-CAA hybrid computations. *Left side: instantaneous perturbed fields obtained via the CFD calculation of the isolated TC (top) and the subsequent CFD-CAA computation of the QFF-installed TC (bottom). Right side, bottom: deltas (in dB) between the Sound Pressure Level fields associated with the isolated and the QFF-installed configurations, as recorded within two lateral planes (xy and yz). Right side, top: Power Spectral Density of the acoustic pressure radiated in the far-field (QFF-installed TC in red, isolated TC in black. In black dashes, the isolated TC result obtained via CFD-FWH).*

The primary conclusion of this study was that the total magnitude of the installation effects associated with the TC model in the QFF was rather modest. In particular, at the 6 microphone locations used during testing, the installation effects led to amplitude differences of less than 40% in magnitude (with a change in amplitude varying between –1.35 dB and +3.45 dB, depending on the microphone location). Most of these effects were due to the QFF components themselves, resulting either from the confinement of the acoustic emission by side plates, or from additional reflection / diffraction of radiated waves by both the collector plate and the nozzle. Very slight modifications were due to the QFF jet flow, which mainly resulted from convection being restricted to the region of the jet. More details about this study, which outcomes are too numerous to be included here, can be found in Ref. 12.

Obviously, the conclusions drawn in this study are valid only for the configuration that had been assessed here, and could not be generalized to other QFF experiments, especially those involving noise sources that differ greatly from the low-frequency, dipole dominated noise radiation associated with the TC configuration. In particular, considering the relatively high frequencies characterizing usual airframe noise sources, most QFF acoustic experiments should be more strongly influenced by the diffraction across the shear layers surrounding the QFF jet flow.

For this reason, more recently, a complementary work was conducted jointly by Onera and NASA, so as to extend this investigation to include higher frequency sources, in order to provide a more complete numerical assessment of the installation effects characterizing the QFF facility, among which i) the convection/refraction

effects associated with the spreading of the QFF jet, and ii) the reflection/diffraction effects induced by some of the QFF constitutive devices. The present paper outlines such work that should help further assess the acoustic installation effects that may be important in the type of testing typically done in the NASA LARC's QFF facility.

III. Numerical Assessment of Acoustic Installation Effects by QFF onto Synthetic TC Noise Emission, via CAA Calculations based on an Equivalent Dipole Source

A. Computational Strategy and Means

Although CFD-CAA hybrid calculations offer a higher degree of realism to the noise prediction, in some cases, pure CAA calculations based on elementary sources may enable interesting qualitative studies to be achieved at a much more reasonable cost[7]. This only requires that enough information is known about the noise generation stage for equivalent sources are analytically synthesized, based on the characteristics (location, frequency, relative magnitude, etc.) of the acoustic emission. On that stage, one can recall that experiments conducted within QFF mostly concern airframe noise, which sources can generally be decomposed into either monopoles (e.g., thickness noise) or dipoles (e.g., loading noise) emitting at a given tonal frequency. Therefore, in order to ease the present numerical assessment of acoustic installation effects by the QFF environment onto other types of noise emissions, it was decided to solely perform CAA computations based on an equivalent tonal source, with the latter to be constituted with either a monopole or a dipole.

All CAA calculations were performed with ONERA's *sAbrinA* solver[4-7], which is a structured, time-accurate CAA code that solves either the full or the linear Euler equations, in a conservative or perturbed form. The solver employs high-order, finite-difference operators, involving 6^{th}-order spatial derivatives and 10^{th}-order filters, as well as a 3^{rd}-order, multi-stage, Runge-Kutta time-marching scheme. The code deals with multi-block structured grids with one-to-one interfaces, and is fully parallelized using the Message Passing Interface (MPI) standard. Finally, the solver includes the usual boundary conditions (reflection by solid walls, non-reflecting / free-field radiation, etc.), as well as some unique to specific applications. More detailed information about the *sAbrinA* solver and its underlying methodology can be found in Refs. 8-11.

B. Numerical Assessement of Acoustic Installation Effects by QFF onto a synthetic TC Noise Emission

In order to check the relevance of the numerical strategy envisaged here (i.e. CAA calculations based on equivalent sources), a preliminary study was first conducted, so as to assess the coherency of results obtained with respect to those acquired with the help of a higher fidelity approach, that is, via CFD-CAA hybrid calculations (i.e. based on a realistic source). With that view, the *QFF-installed TC within a free flow* configuration addressed in Ref. 12 was CAA-computed, the realistic source (derived from CFD data) being here replaced with a simplistic source of dipolar nature. Such an equivalent dipole was synthesized directly within the CAA solver, with the help of two harmonic monopoles in phase opposition. The latter monopoles were located one aside the other, both being allotted a same frequency (f'_{prim}, corresponding to the TC primary shedding) and assigned an identical (arbitrary) amplitude. This synthesized dipole source was positioned nearby the downstream cylinder, and centered in the mid-span plane (behaving thus as a fixed source, whereas the real source was somehow travelling slowly along the span – see Ref. 12).

The CAA calculation was run for a physical time duration equaling a total of 8 source periods ($T_{prim} = 1/f'_{prim}$), which was sufficient for a stationary state to establish itself all over the computational domain. One can here notice that such time duration was 2.5 times shorter than the one of the CFD-CAA calculations based on the realistic source (see Ref. 12). This is due to the fact that the present CAA calculation involved an acoustic source that i) was solely composed of harmonic content (i.e. did not include any other spectral components than the low frequency f'_{prim} one) and ii) was located at a fixed position (i.e. was not traveling along the span). The bottom of Figure 3 (and 4, respectively) plots the instantaneous (and Root Mean Square) perturbed pressure field obtained at the end of the present *equivalent source*-based CAA calculation, whereas top of the same Fig. 3 (resp. 4) provides the results coming from the *realistic source*-based CFD-CAA hybrid calculation of Ref. 12. When comparing these plots, one can appreciate how both results are very similar, at least from a qualitative point of view (levels were adjusted, because of the arbitrary amplitude given to the equivalent source). In particular, one can see how all patterns match quite well over the whole domain, to the exception of the source region, over which outputs differ more noticeably - as was to be expected.

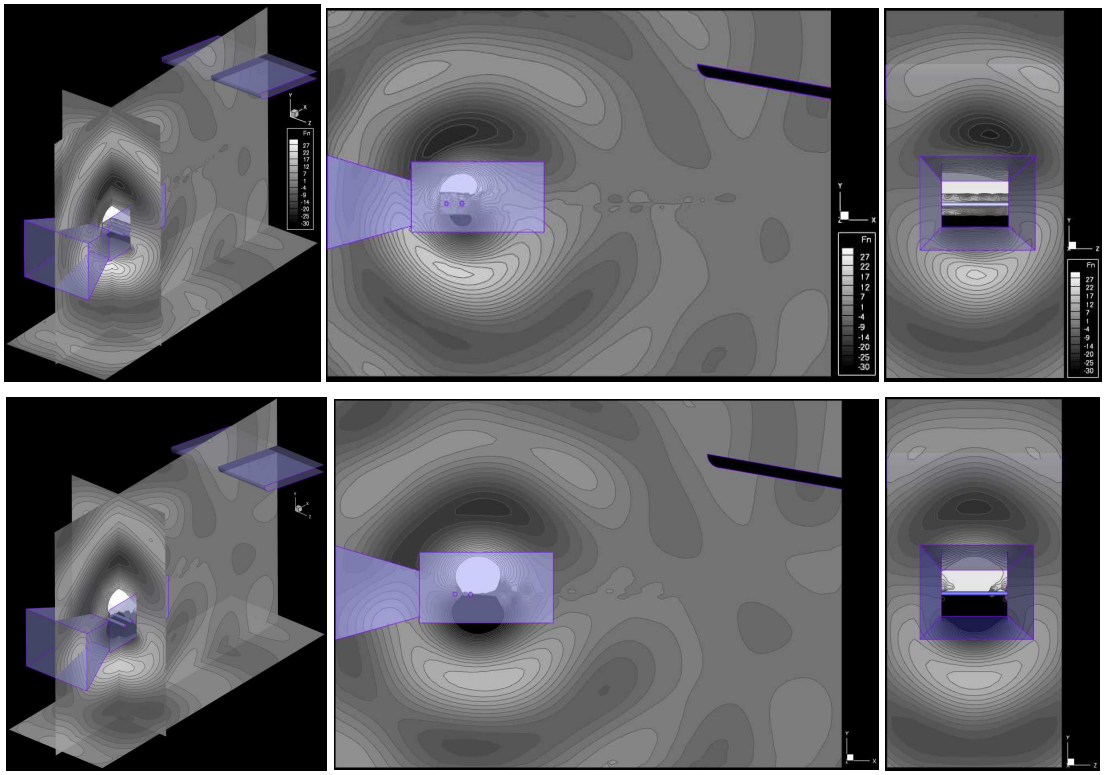

Figure 3. Numerical Assessement of Acoustic Installation Effects by QFF onto a TC Noise Emission, *via either a CFD-CAA hybrid computation (top) or an equivalent source-based CAA calculation (bottom). Instantaneous perturbed pressure field (in Pa, with amplitude levels adjusted), as recorded within both xy (left and center) and yz (left and right) planes.*

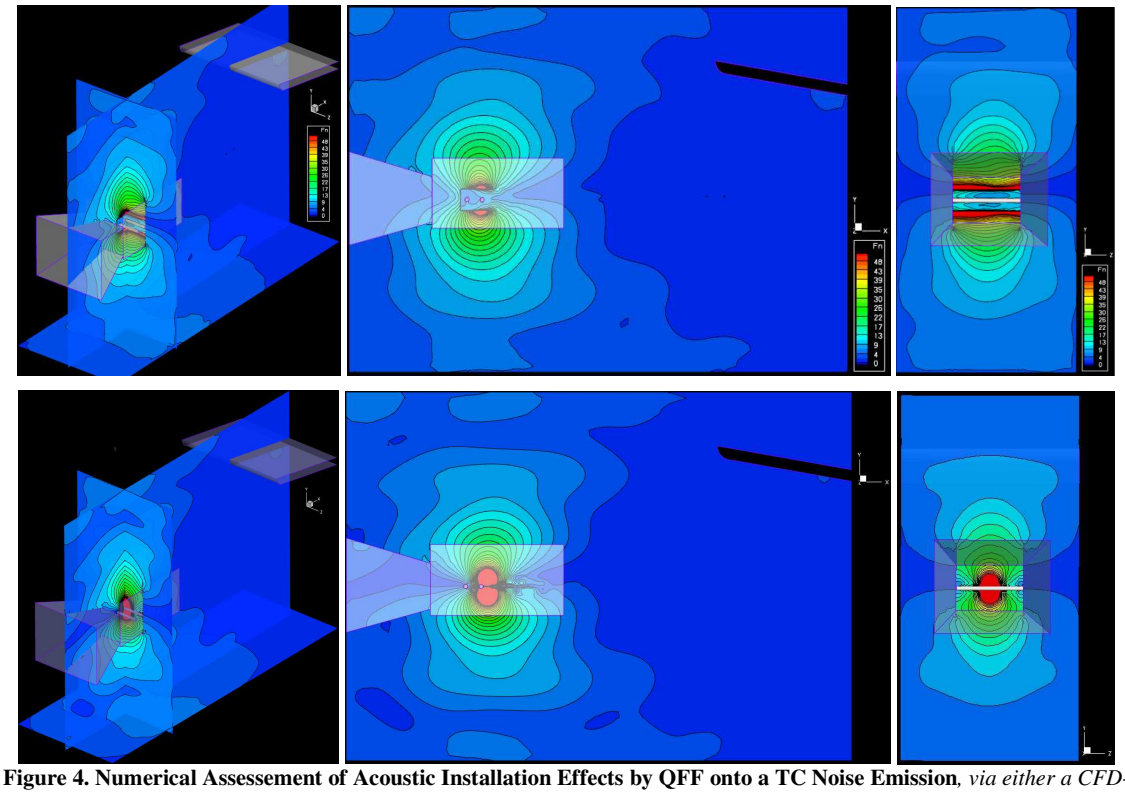

Figure 4. Numerical Assessement of Acoustic Installation Effects by QFF onto a TC Noise Emission, *via either a CFD-CAA hybrid computation (top) or an equivalent source-based CAA calculation (bottom). RMS perturbed pressure field (in Pa, with amplitude levels adjusted), as recorded within both xy (left and center) and yz (left and right) planes.*

Regarding quantitative aspects, the assessment of installation effects by the QFF apparatus was achieved in the same way as was done in Ref. 12. To this end, the previous QFF-installed TC configuration was reduced into a (quasi) isolated TC, with all QFF devices removed (and replaced with only two minimal side plates, see Ref. 12 for more details). The equivalent source-based CAA calculation of such a quasi-isolated TC configuration was then conducted, delivering outputs from which the QFF acoustic installation effects were finally assessed. The latter effects were obtained by subtracting the Sound Pressure Level field associated with the quasi isolated TC configuration from the one characterizing the QFF-installed TC, highlighting thus the cumulative acoustic installation effects by the QFF apparatus (side plates, collector plate and nozzle). As one can see in Fig. 5, the resulting acoustic patterns are here very similar to the ones obtained via the CFD-CAA hybrid calculation based on the realistic source (see right bottom of Fig. 2). The main difference between both results is that, compared to the latter CFD-CAA hybrid calculation case, the delta effects are now perfectly symmetric with respect to the mid span central plane. This is due to the fact that, compared to the realistic one, the equivalent source is more compact and does not evolve along the span; therefore, it does not interact with the side plates, in contrast to what happened in the real source case. Apart from that, all the trends that had been previously observed through the realistic source based CFD-CAA coupled calculation are here globally well recovered. In particular, the overall acoustic installation effects produced by the QFF devices onto the low frequency dipole source addressed here are quite close to the ones acting onto the realistic TC source, with amplitude differences that do not exceed $3dB$ (that is, 40%) at the microphone locations where the TC experimental data were acquired (see Ref. 12).

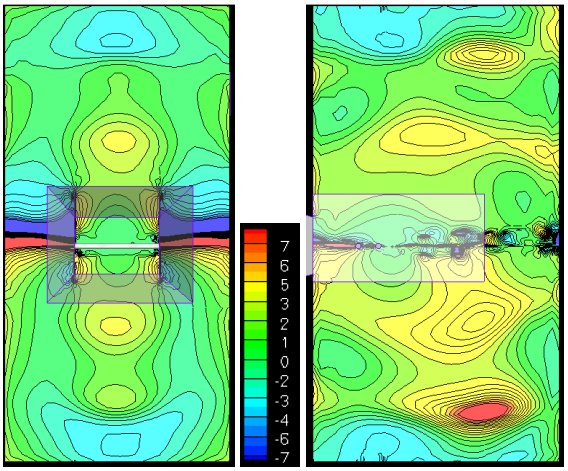

Figure 5. Numerical Assessement of Acoustic Installation Effects by QFF onto a synthetic TC Noise Emission, *via an equivalent source-based CAA calculation. Deltas (in dB) between the Sound Pressure Level fields associated with the isolated and the QFF-installed configurations, as recorded within two lateral planes (xy and yz).*

From a methodological point of view, this tends to confirm that the present TC configuration seems to be adequately modeled by simple equivalent sources. Indeed, the present conclusions and even the quantitative numbers are consistent with those previously provided by NASA/LARC researchers in their earlier assessment of QFF installation effects, achieved using an Equivalent Source Method (ESM) forced by equivalent dipoles[15].

C. Further Investigation of Installation Effects using Synthetic TC Noise

With the view of going further in such an assessment of acoustic installation effects by the QFF apparatus onto the TC emission, two alternative equivalent source-based CAA calculations were then conducted. These two calculations directly benefitted from the simpler structure of the equivalent source, whose compact character allowed the complete removal of the QFF devices (e.g. the minimal side plates – see the dedicated discussion in Ref. 12), leading to a fully (rather than a quasi) isolated TC configuration. For these two alternative calculations, the dipole equivalent source was thus considered as emitting within a medium free of any solid element. The latter medium was taken as homogeneous, being first considered as quiescent, before a uniform mean flow was imposed with a Mach number that was adjusted to the freestream value of the TC configuration ($M = M_\infty$ = 0.166). All results coming from the two previous and these two additional CAA calculations are depicted in Figures 6 and 7, which respectively plot the instantaneous and the RMS (Root Mean Square) perturbed pressure fields obtained after a stationary state had been reached all over the domain.

First of all, one can notice that the outputs associated with the radiation of the dipole equivalent source within an infinite medium at rest (see Figs. 6-a and 7-a) deliver an indirect check of the CAA method and computational set up employed here. In particular, one can see that the acoustic radiation is effectively that of a dipole of frequency f'_{prim} (with a wavelength λ of approximately $28D$, with D the cylinders' diameter – see Ref. 12), and that no noticeable spurious reflection effects by the outer boundaries of the computational domain are visible. Now, by comparing these last results with the ones associated with the dipole emission within a uniform flow (see Figs. 6-b and 7-b), one can see how much the convection effects by the mean flow modify the radiation patterns in the xy plane, by compressing (or expanding) the acoustic waves and reinforcing (or decreasing) their levels in the upstream (downstream) direction. The results confirm the observations that had been made with the help of the CFD-CAA hybrid calculation of Ref. 12, regarding the mean flow effects on the realistic TC source emission.

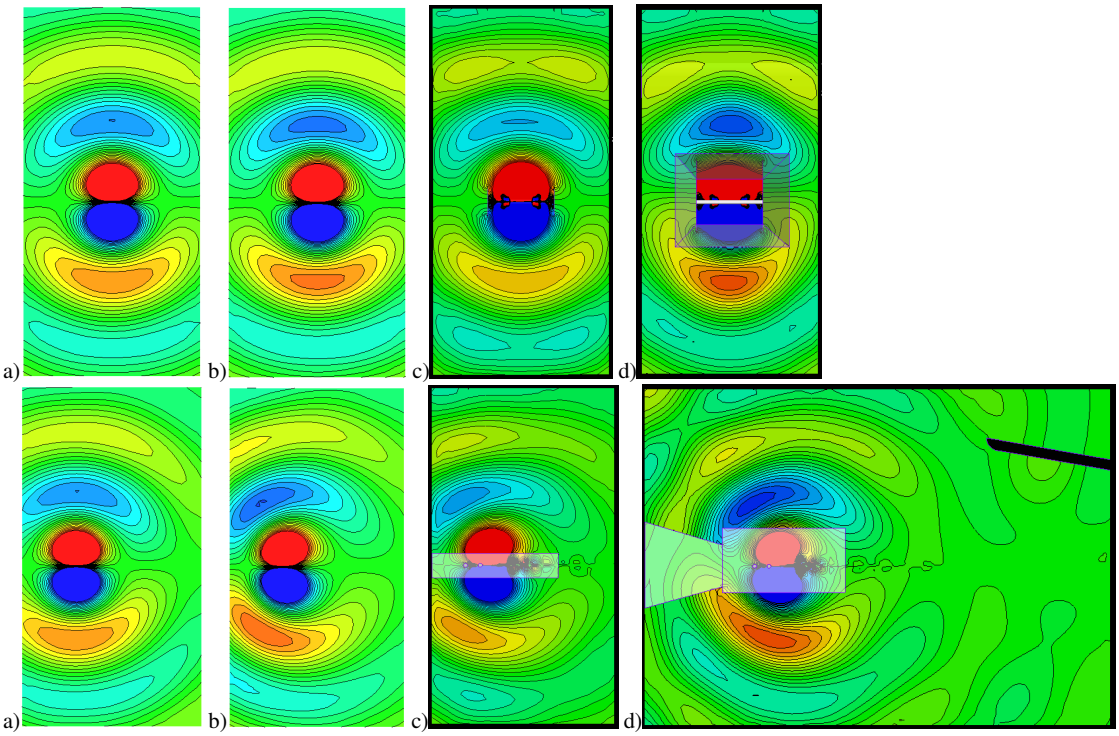

Figure 6. Numerical Assessement of Acoustic Installation Effects by QFF onto a synthetic TC Noise Emission, *via equivalent source-based CAA calculations. Instantaneous perturbed pressure field (Pa), as recorded within both xy (bottom) and yz (top) planes. From left to right; dipole source emitting within either a medium at rest (a) or a uniform flow (b) with no obstacle, as well as in the presence of the quasi isolated (c) or the fully QFF-installed (d) TC with associated jet flows.*

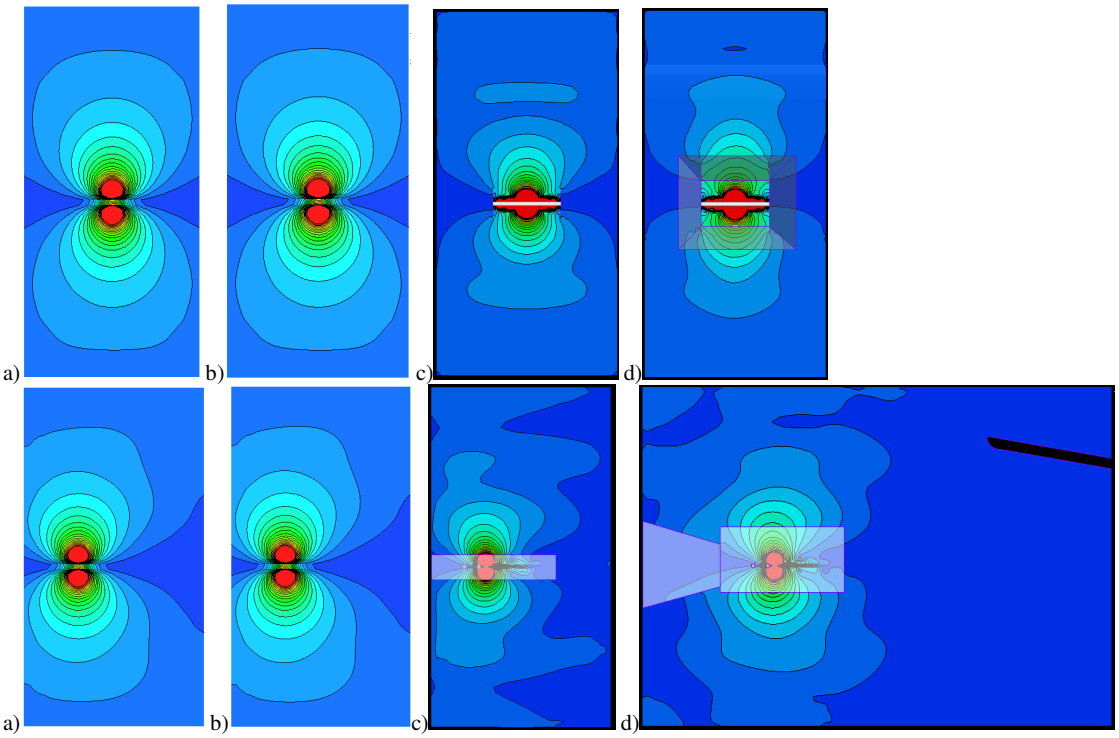

Figure 7. Numerical Assessement of Acoustic Installation Effects by QFF onto a synthetic TC Noise Emission, *via equivalent source-based CAA calculations. RMS perturbed pressure field (Pa), as recorded within both xy (bottom) and yz (top) planes. From left to right; dipole source emitting within either a medium at rest (a) or a uniform flow (b) with no obstacle, as well as in the presence of the quasi isolated (c) or the fully QFF-installed (d) TC with associated jet flows.*

By comparing the latter (free-field radiation) results against the ones acquired for the quasi isolated TC configuration (see Figs. 6-c and 7-c), one can then appreciate how, although they are relatively small, the minimal lateral side plates modify the acoustic emission in a non negligible manner. In particular, regarding more what happens in the *yz* plane, one can clearly see how the relative confinement such minimal side plates induce on the dipole source leads the latter to emit in an altered manner. From a modeling point of view, one can notice that such effects by the side plates lead the equivalent source to behave more closely to the realistic (CFD) one (compare for instance Fig. 6-c and 7-c with Fig. 4). Finally, when comparing the latter quasi-isolated TC outputs with the ones given by the QFF-installed TC configuration (see Figs. 6-d and 7-d), one can see how the QFF devices and jet flow alter further the dipole noise emission and propagation, leading the cumulated effects by the QFF installation onto the TC noise radiation to be globally recovered, as underlined in the previous section.

D. Intermediate Conclusions

From what precedes, one can conclude that, even if it is based on an equivalent (and, thus, less accurate) source, a CAA calculation reproduces fairly accurately the acoustic installation effects induced by the QFF environment. One can thus infer that, regarding problems close enough to this one (e.g. involving a dipole source of low frequency), the QFF acoustic installation effects could be properly investigated with the help of typical acoustic methods (such as CAA, ESM[15], or BEM), with the latter to be based on equivalent simplistic sources. This is an important outcome since it indicates that, in some cases, there would be no need for performing more advanced (and, thus, expensive) computations, including those of preliminary nature that only seek to derive suitable source data for input to acoustic extrapolation methods (FWH or CAA). In addition, even for situations where CFD data are available (such as was the case, here), pure CAA computations based on equivalent sources could advantageously replace those based on more realistic simulations (i.e. CFD data), which are more computationally intensive (with extra CPU costs associated with the CFD-CAA coupling operations, as well as a possibly increased physical time needed for achieving a stationary state, etc.). As an illustration of that last point, one can notice that, thanks to the fact they were both less expensive to compute (CPU cost, etc.) and easier to handle (purely isolated configuration, etc.), compared to the CFD-CAA computations of Ref. 12, the present equivalent source-based CAA calculations allowed the investigation of acoustic installation effects by the QFF environment to be completed further in an easy and straightforward manner.

On this stage, however, it is important to underline that the present investigation also shows how far the fidelity of CAA calculations based on an equivalent source strongly depend on the latter, whose *characteristics* and *behavior must be as close as possible* from the real sources. Therefore, except for particular situations where the physical source is sufficiently known to be efficiently modeled with simplistic sources, there might be no other alternative than to make use of more advanced computational means relying on both CFD *and* CAA approaches. In particular, from what precedes, one can conclude that the CFD-CAA hybrid methodology employed in Ref. 12 seems to be as appropriate for evaluating installation effects as other and simpler computational approaches, while allowing the possibility of including further realism (source description, refraction effects, etc.).

IV. Further Numerical Assessment of Acoustic Installation Effects by QFF onto Airframe Noise Emissions, via CAA Calculations based on Equivalent Multi-Tonal Monopole Sources

It must be pointed out again that all the previous conclusions are valid only for the TC configuration that was addressed here, and should not be generalized to other QFF experiments, especially those involving noise sources that differ noticeably from the low-frequency dipole one investigated here.

In particular, regarding the sole refraction effects by the sheared / confined jet flow characterizing the QFF facility, one can here recall that dedicated investigations[12] permitted the identification of the very slight impact that the QFF jet flow shear layers had on the TC noise emission, which was much more affected by the other QFF artifacts (e.g., reflection / diffraction by the apparatus). As stated in Ref. 12, such a conclusion must be tempered by the fact that the TC noise source is of very low frequency, which renders it almost insensitive to refraction effects by the jet shear layers. Such a situation is quite unusual because the small scale of experimental models leads to noise emission at very high frequency (50 kHz is not rare).

With the view of investigating that point further, a dedicated study was conducted within the present framework, through additional CAA simulations based on simplistic equivalent sources at higher frequencies. In particular, one objective here was to isolate the refraction/convection effects by QFF jet flow from the reflection/diffraction ones induced by the experimental apparatus, so that their relative weight onto sources of various frequencies can be estimated.

A. Computational Strategy and Set-Up

As for what was done previously (see Section III), CAA computations achieved here were based on an

equivalent source, of simplistic nature. Such acoustic excitation, however, was no longer taken as a pure harmonic dipole, but as *multi-tonal* monopoles; more precisely, the source point was defined as a sum of 8 monopoles, each being allotted an arbitrary amplitude and a particular frequency corresponding to a multiple of a given fundamental one. The latter fundamental frequency was set to $f_1 = 1.115\ kHz$ (i.e. $f_1 \sim 5f'_{prim}$) so that its associated wavelength[*] equals $\lambda_1 = H$ (with H the half-height of the test section[†]). Each one of the 7 other tones (source's harmonics) had a frequency given by $f_n = n \times f_1$ with n the number of tone considered (i.e. $f_{2,3,\ldots,8} = 2.23\ kHz,\ldots, 8.92\ kHz$), that is, was associated with a wavelength of $\lambda_n = H/n$ (i.e. $\lambda_{2,3,\ldots,8} = H/2,\ldots, H/8$).

On this stage, one can precise that privileging moderate to high frequencies sources was made on purpose, in order to examine the relative weight that installation effects may have onto acoustic waves of small wavelengths / high frequencies, which are often of more relevance to small-scale wind tunnel testing. Indeed, in the present case, the upper harmonic source (8th tone) exhibited a frequency of almost $9kHz$ ($f_8 \sim 40f'_{prim}$), a value that is not far away from the $10kHz$ upper limit beyond which, for the present flow configuration, other phenomena may arise (which cannot be easily reproduced by CAA, e.g. diffusion by small scale turbulence). Additionally, one can also precise that specifying these multi-tonal sources as pure harmonics of a fundamental one was also made on purpose, in order to enable simulating them in one shot, via a single time domain CAA calculation (to be post-processed through Fourier transforms in time, delivering then each source respective contribution to the overall radiation field).

Finally, compared to what was done for the previous TC case, the present (multi-tonal monopoles) source was located further downstream on the jet axis, at a distance of 42" (i.e. approx. $3.5H$) from the nozzle exit (a location that is more representative of what may be encountered in airframe noise experiments conducted in QFF[‡]).

Regarding now the jet mean flow to be considered for the CAA consumption, the background pressure field was taken as homogeneous, with a nominal value corresponding to atmospheric conditions ($P_o = 101325\ Pa$). In contrast, the background velocity and density fields were taken as heterogeneous. More precisely, the velocity field was prescribed a jet profile, which was derived with the help of similarity functions (see Ref. 12). Such velocity profile was driven by both i) the Mach ratio M_r between Mach numbers in the jet core and at infinity ($M_r = M_\infty/M_{core}$) and by ii) the spreading angle (α) of the jet's mixing layers. On another hand, the density field was derived via the Crocco-Buseman relation, which relates the local temperature to the velocity. Such density field was thus not only driven by the Mach ratio (M_r), but also by the temperature ratio T_r between the temperature in the jet core and at infinity ($T_r = T_\infty/T_{core}$). All these flow parameters were adjusted to the nominal values usually recorded within the QFF; in particular, the Mach numbers at infinity and within the jet core were respectively set to $M_\infty = 0.0$ and $M_{core} = 0.17$ (corresponding thus to a QFF experiment run with the highest possible flow speed condition, whilst leading to a zero M_r ratio). On another hand, the temperatures at infinity and in the jet core were respectively set to $T_\infty = 67°F$ (i.e. $293K$) and $T_{core} = 83°F$ (i.e. $301.5K$, corresponding thus to a QFF experiment achieved during a hot summer day, whilst leading to a T_r of 0.973[§]). Based on the previous parameters, the jet mean flow was prescribed both density and velocity profiles, with a boundary layer thickness of initial value 0.6" (i.e. $H/20$) and a spreading angle α of 7° (i.e. providing a spreading mixing layer).

As was said, the objective here was to assess not only the convection/refraction effects by QFF jet flow but also the reflection/diffraction effects by the facility solid devices; therefore, as had been done for the TC case, the present configuration included part of the QFF installation. In contrast to what was done in the previous section, however, the QFF installation devices were here restricted to the sole side plates, which were considered as i) infinitely thin and ii) symmetric with respect to the xz plane. The reason for not accounting more accurately for the QFF set up (which has side plates that are thick and asymmetric) was to save computational resources (see below). Here, one can notice that the jet flow was analytically adjusted in the same way as what had been achieved in Ref. 12, so that the flow is consistent with the side plates presence, resulting in a *confined* (and, thus, no longer free) sheared jet.

In order to save computational resources, benefit was taken from the double symmetry offered by this configuration with respect to the xy and xz planes. Therefore, only one quarter of the QFF environment was meshed, which was achieved thanks to a unique CAA grid. The latter was generated following precise meshing criteria, which were driven by the double need of i) a sufficient discretization of acoustic waves (especially those

[*] Towards the yz plane, i.e. free of any Doppler effect.

[†] One can here recall that the dimensions of QFF test section are $2H \times 3H$, with $H = 12$".

[‡] In QFF, models are usually positioned at a location that ranges from $2H$ to $4H$, with H the half height of the jet. In the TC experiment, the downstream cylinder centroid was located at a distance of 27.3" (i.e. approx. $2.275H$) from the nozzle exit. In other experiments (such as those addressing trailing edge of flap side edge noises, but not only[21]), the typical location is 40" (i.e. approx. $3.3H$) from the nozzle exit.

[§] Indeed, the QFF jet is roughly isothermal, since the temperature of test chamber is constant (approx. 70°F) all year long, whereas the jet core temperature is that of the atmosphere outside the building. This leads to a maximum difference of temperatures in and outside the jet of ± 15°F (i.e. 3%, in terms of ratio T_r).

of higher frequency, e.g. f_8 tone) all over the domain and ii) a decent mesh resolution within the jet shear layers areas. In particular, an automatic grid refinement (based on the Malesh transform) was applied over the sheared flow region, ensuring that at least 12 to 15 grid points were present in the mixing layers (especially upstream the computational domain, i.e. nearby the nozzle exit, where QFF mixing layers' thickness goes down to the boundary layer initial value, that is, 0.6" i.e. *H*/20). This resulted in a heterogeneous Cartesian monoblock of $482 \times 211 \times 205$ (i.e. approx. 21.3 millions) points, which extended up to a distance of 100" (i.e. 8.5*H*) in the jet axis and 50" (4.25*H*) in the two lateral directions[*].

As an illustration of the computational set-up, Fig. 8 displays a view of the CAA domain and mean flow that were derived and used for the CAA consumption; as one can see, the sheared jet flow is partly confined within the side plates, which extend downstream the nozzle exit (up to a distance of approx. 70", i.e. 6*H*). As one can also see, thanks to the double symmetry of the configuration addressed here, the computational domain comprises only a restricted area of the space ($x > 0$; $y > 0$; $z > 0$), including solely one side plate's upper part (the nozzle and collector were here drawn for illustrative purposes only).

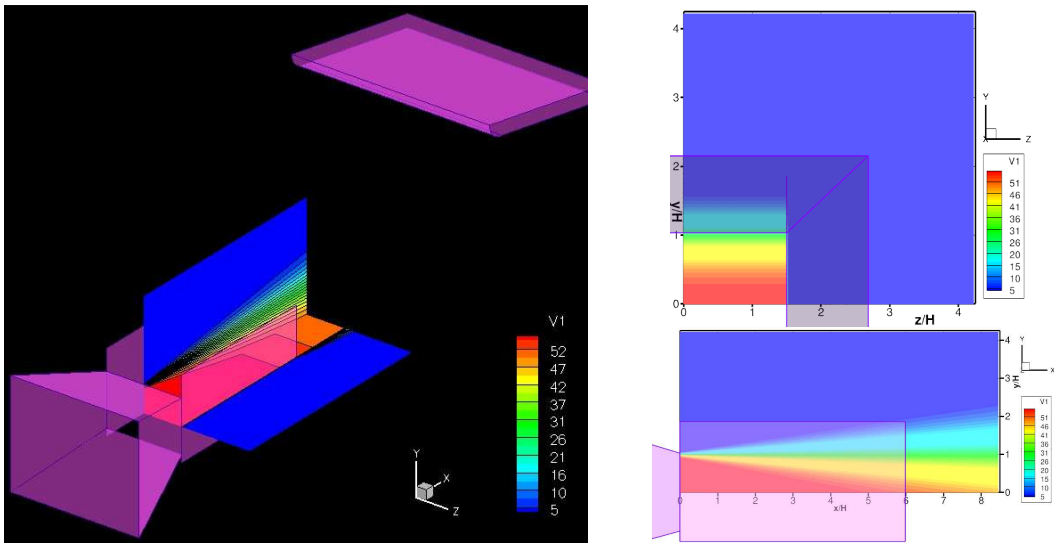

Figure 8. Numerical Assessement of Acoustic Installation Effects by QFF onto synthetic Airframe Noise Emissions, via *CAA calculations based on an equivalent monopole source emitting at various frequencies (from f_1 =1.115 kHz to f_8 = 8.92 kHz) within QFF environment. Mean flow (axial velocity) associated with QFF (sheared jet confined within thin and symmetric side plates, here colored in purple). 3D view (left side) and lateral cuts (right side) along the xy (top) and yz (bottom) half-planes passing by the source. QFF nozzle and collector are here drawn for indicative purpose only.*

Once such grid + flow inputs were processed for parallel computing, the CAA calculation was run over 468 cores of Onera's super computer. Simulation was run until a stationary state has established all over the computational domain, which required a physical duration of 8 (resp. 64) times the period associated with the fundamental (resp. 8[th]) tone emitted. The time step used in the simulation was such that the corresponding temporal discretization was of 200 (resp. 25) iterations per period. Thanks to the number of cores used, this CAA calculation (of 21 million of grid points / 1600 iterations) was completed in less than 2 hours of wall-clock time.

On this stage, it is worth mentioning that for CAA-solving a problem as this one with the help of the 7-point stencil / 6[th] order standard FD (Finite Difference) schemes *sAbrinA* solver usually relies on, a much denser grid (of more than 200 million cells) would have been required. This is why, here, use was made of the so-called *Intrinsically Optimized Finite Differences* (IOFD) schemes[17], a new class of optimized FD propagation schemes that were recently developed at Onera (Cunha & Redonnet, 2012). One can here recall that such IOFD schemes are of very high accuracy[†], thanks to an optimization process that is based on a minimization of the scheme's

[*] One can here notice that such a domain extent was large enough for ensuring propagation up to some of the near-field microphones associated with the MADA (Medium Aperture Directional Array) experimental data acquisition system, which has a boom radius of 60" (i.e. 5*H*);

[†] More precisely, with no more than 4 Points Per Wavelength (PPW), an IOFD scheme of 15-point stencil / 8[th] order guarantees that the error made on the group velocity (from which depends the acoustic energy transport and, thus, the overall accuracy of the CAA stage) is less than 0.1%. Compared to the accuracy of a classical 7-point stencil / 6[th] order standard finite difference scheme[18,19] (which corresponding minimal PPW is 12), this represents a gain of 3 per direction, *i.e.* a factor 27 in 3D. Needless to say, such a benefit can be directly translated into a reduction of the CAA computational grid, with memory needs that are decreased by the same factor, and CPU times that can be reduced even more (down to a factor 54, depending on the CFL constraints).

leading-order truncation error (rather than on an optimization of the scheme' spectral properties, such as usually done[18,19]). These IOFD schemes were previously validated via academic test cases of increasing complexity[17], before they were applied to a practical problem of airframe noise[20], the latter of which was handled via a CFD-CAA hybrid calculation relying on IOFD derivative schemes of 15-point stencil (along with IOFD filters of 21-point stencil). In the present case, the same 15- (resp. 21-) point stencil IOFD derivative (resp. filter) schemes were employed, which permitted a much smaller CAA grid to be used (inducing thus reduced calculation CPU time, etc.), compared to what would have been required if regular 7- (resp. 10-) point stencil standard FD derivative (resp. filter) schemes had been used instead.

B. Numerical Assessment of Acoustic Installation Effects by QFF onto Airframe Noise Emissions, via CAA Calculations based on Equivalent Multi-Tonal Monopole Sources

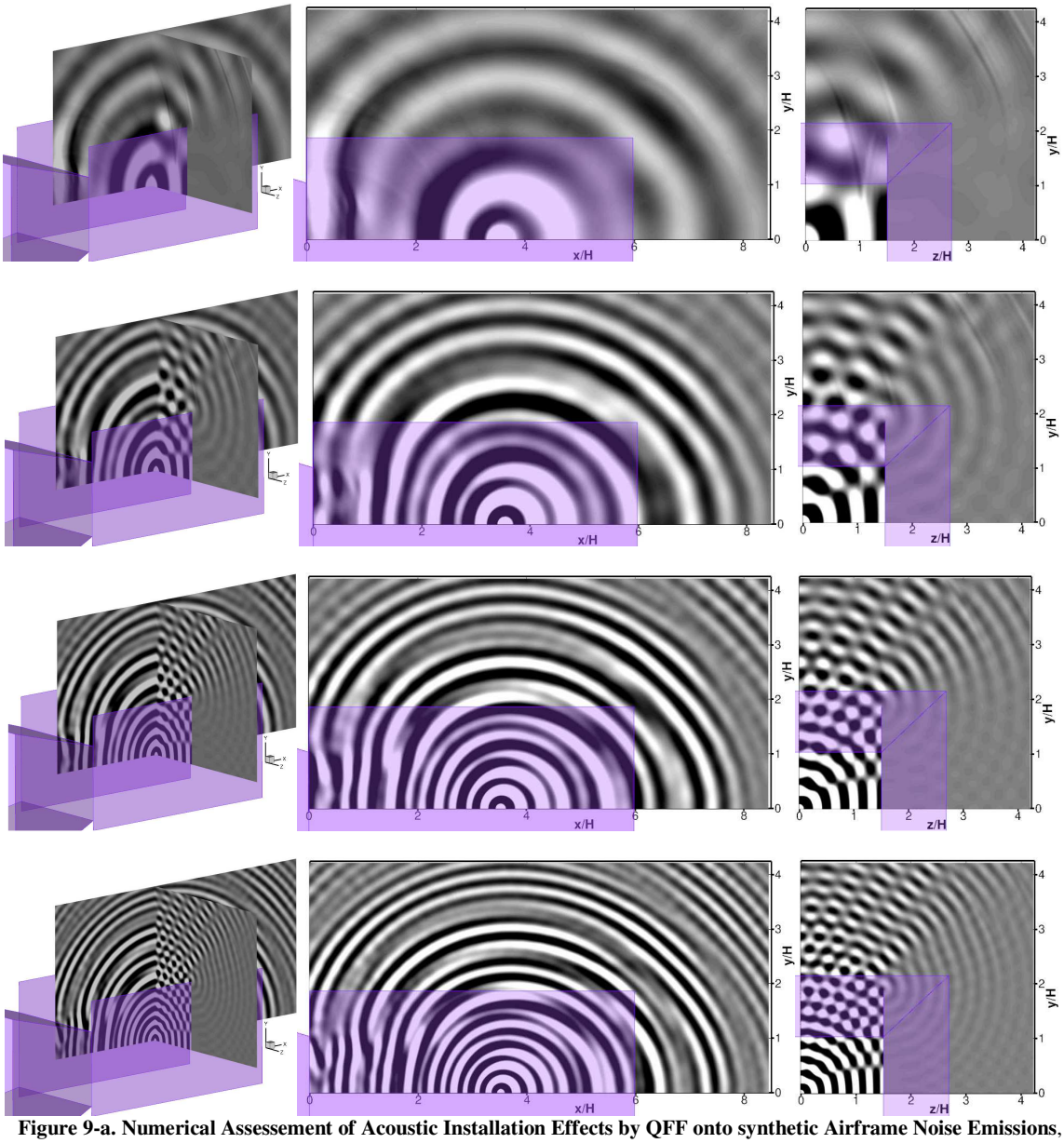

Figure 9-a. Numerical Assessement of Acoustic Installation Effects by QFF onto synthetic Airframe Noise Emissions, via *CAA calculations based on an equivalent monopole source emitting at various frequencies (from f_1 =1.115 kHz to f_8 = 8.92 kHz) within QFF environment: calculation case #1 (side plates, jet flow). Instantaneous perturbed pressure field radiated by sources of frequency f_1 to f_4 (from top to bottom). 3D views (left), and lateral cuts along the xy (center) and yz (right) half-planes passing by the source. QFF nozzle is here drawn for indicative purpose only.*

Results of the simulation are presented in Fig. 9-a and 9-b, which display several views of the instantaneous perturbed pressure field obtained at the end of the calculation. As was said, the latter calculation was suitably post-processed (by the means of Fourier transforms in time), so as to isolate the respective acoustic radiation associated with each one of the 8 tonal monopole sources. As one can see, for each source, acoustic waves are importantly altered by the QFF environment, despite of the fact they were initially emitted in a pure isotropic fashion (especially considering their more compact character, compared to the very low frequency equivalent source used for the TC case addressed previously – see the dedicated discussion in section III.C). Such an altered propagation of acoustic waves is obviously due to the cumulated effects of reflection/diffraction by the side plates and convection/refraction by the jet flow. As a result, each acoustic field exhibits strong interaction patterns and a rather directive signature, two tendencies that become more and more proeminent as the source frequency increases.

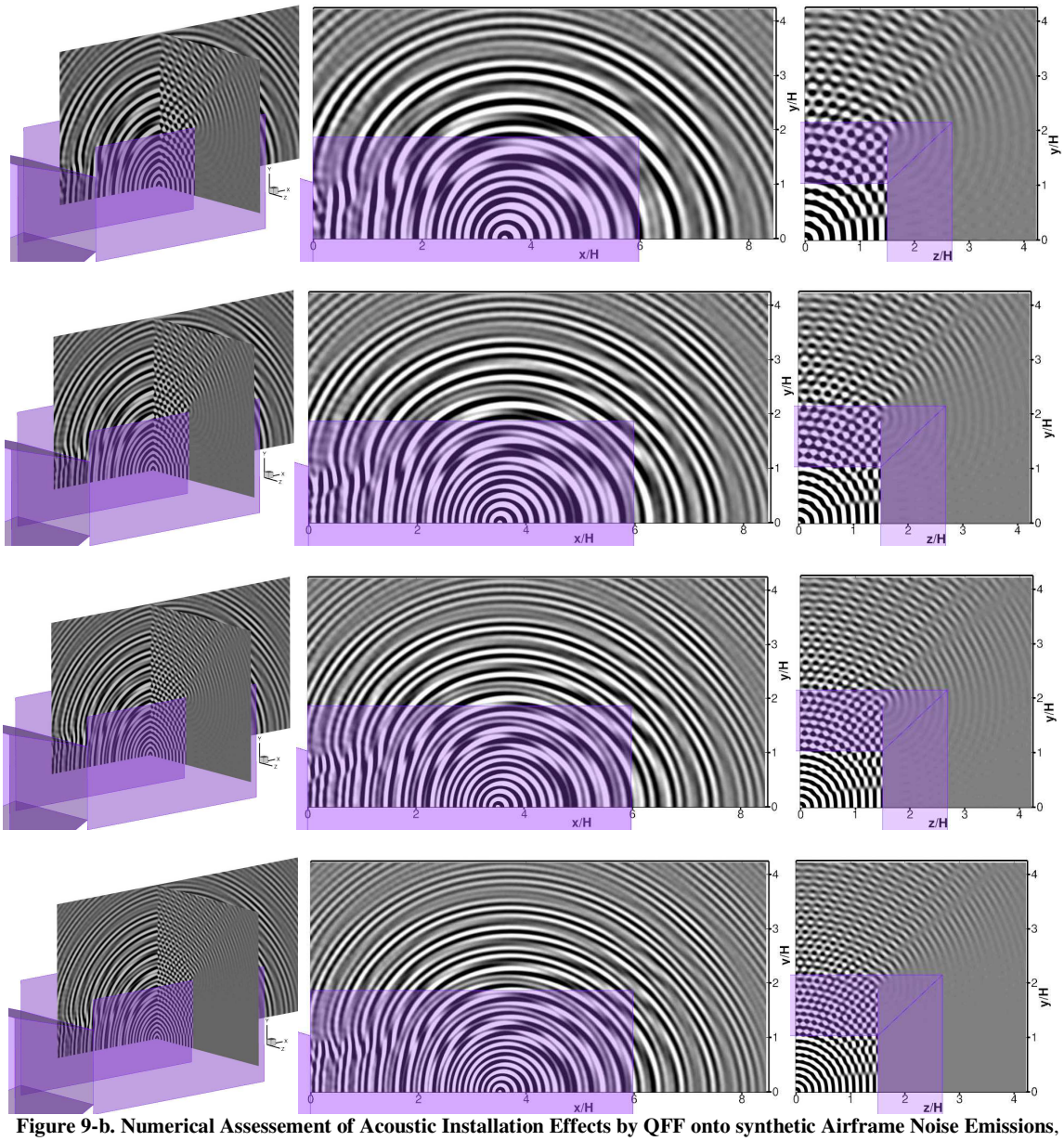

Figure 9-b. Numerical Assessement of Acoustic Installation Effects by QFF onto synthetic Airframe Noise Emissions, via *CAA calculations based on an equivalent monopole source emitting at various frequencies (from f_1 =1.115 kHz to f_8 = 8.92 kHz) within QFF environment: calculation case #1 (side plates, jet flow). Instantaneous snapshot of the perturbed pressure field radiated by sources of frequency f_5 to f_8 (from top to bottom). 3D views (left), and lateral cuts along the xy (center) and yz (right) half-planes passing by the source. QFF nozzle is here drawn for indicative purpose only.*

Among other things, for all 8 sources, one can observe how the reflection by the side plates induces a secondary emission, which interacts importantly with the primary one. All of these primary and secondary acoustic waves end up in constructing complex interaction patterns, with either phase reinforcement or cancellation effects.

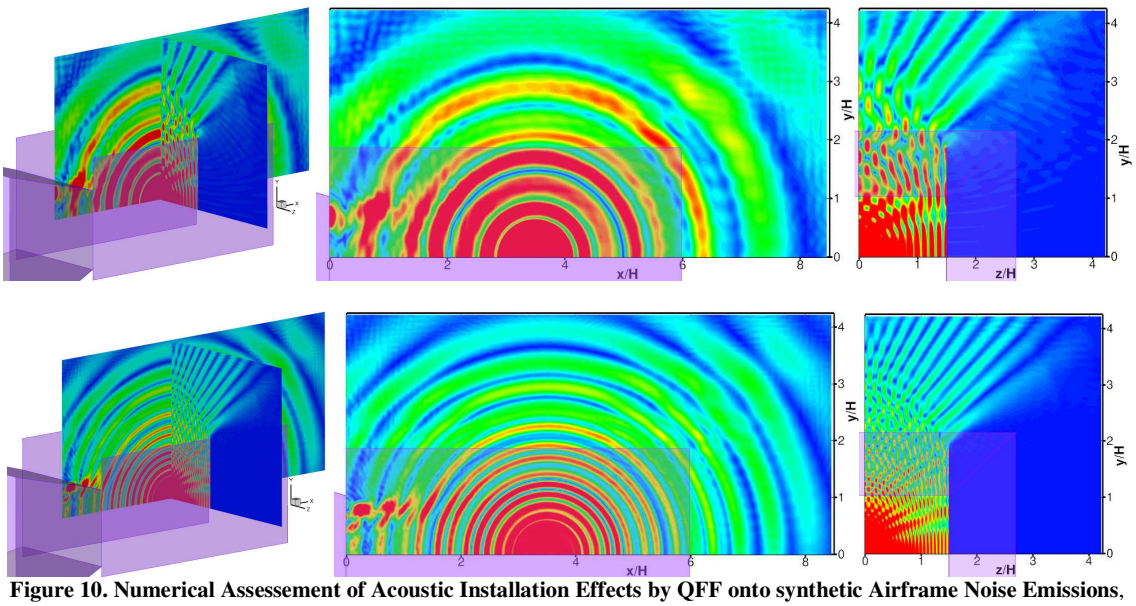

Figure 10. Numerical Assessement of Acoustic Installation Effects by QFF onto synthetic Airframe Noise Emissions, via *CAA calculations based on an equivalent monopole source emitting at various frequencies (from f_1 =1.115 kHz to f_8 = 8.92 kHz) within QFF environment : calculation case #1 (side plates, jet flow). RMS map of the perturbed pressure field radiated by sources of frequency f_4 (top) and f_8 (bottom). 3D views (left), and lateral cuts along the xy (center) and yz (right) half-planes passing by the source. QFF nozzle is here drawn for indicative purpose only.*

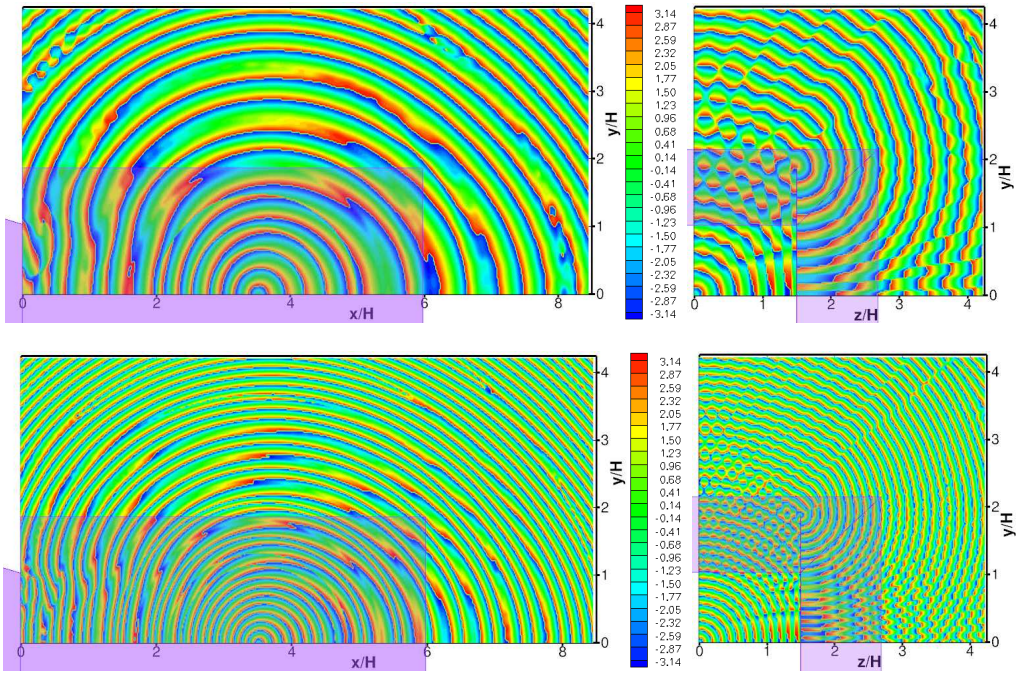

Figure 11. Numerical Assessement of Acoustic Installation Effects by QFF onto synthetic Airframe Noise Emissions, via *CAA calculations based on an equivalent monopole source emitting at various frequencies (from f_1 =1.115 kHz to f_8 = 8.92 kHz) within QFF environment : calculation case #1 (side plates, jet flow). Iso-phase fronts (φ = 0) map of the perturbed pressure field radiated by sources of frequency f_4 (top) and f_8 (bottom). 3D views (left), and lateral cuts along the xy (center) and yz (right) half-planes passing by the source. QFF nozzle is here drawn for indicative purpose only.*

These reinforcement/cancellation effects due to the side plates presence are still more visible on the RMS

maps associated with the previous perturbed fields, as depicted in Fig. 10 (where only the 4th and the 8th tones were displayed, for brevety' sake). There, one can clearly see how its confinement by the side plates makes each source radiating following a very directive manner, with acoustic energy levels that are primarily emitted at the vertical of the test section (that is, towards the near- and far-field microphones locations). Those effects by the side plates are also visible in Fig 11, which plots the iso-phase front maps corresponding to the two previous results; indeed, on the lateral *yz* half-plane (see both right sides of the figure), one can clearly distinguish how most part of these acoustic interaction patterns result from the reflection of wave fronts by the side plates, as well as from their diffraction by the edges of the latter. On another hand, left side of the same Fig. 11 reveals specific patterns that are more likely to be due to refraction effects by the jet flow (see for instance what happens upstream the source, along the shear layer - that is, in the continuity of the nozzle upper side). One can notice how such effects appear to become more proeminent when the source frequency increases.

In order to evaluate how important all these cumulated effects by the QFF side plates and jet flow could be, a second computation was achieved; such calculation corresponded in all points to the previous one, to the exception that the propagation medium was now taken as a free field. The latter was allotted a homogeneous flow of Mach number and temperature values (M_∞, T_∞) equaling the ones previously considered within the jet core (M_{core}, T_{core}). Regarding such 'free-field / uniform flow' calculation, Figures 12, 13 and 14 respectively display the instantaneous, the RMS and the iso-phase fronts maps associated with the perturbed pressure field radiated by either the 4th or the 8th tonal source. As one can see, to the exception of slight convection effects by the mean flow (which Mach number is relatively low, $M_\infty = 0.17$), the sources emission was here left unaltered by the surrounding environment, resulting in acoustic waves radiating following a quasi-isotropic manner. On this stage, and from a more methodological point of view, one can notice that such results validated a posteriori the computational set up and method that were employed for achieving the present study (IOFD derivative and filter schemes, free-field boundary conditions, Fourier transforms-based post-processing, CAA mesh, etc.)

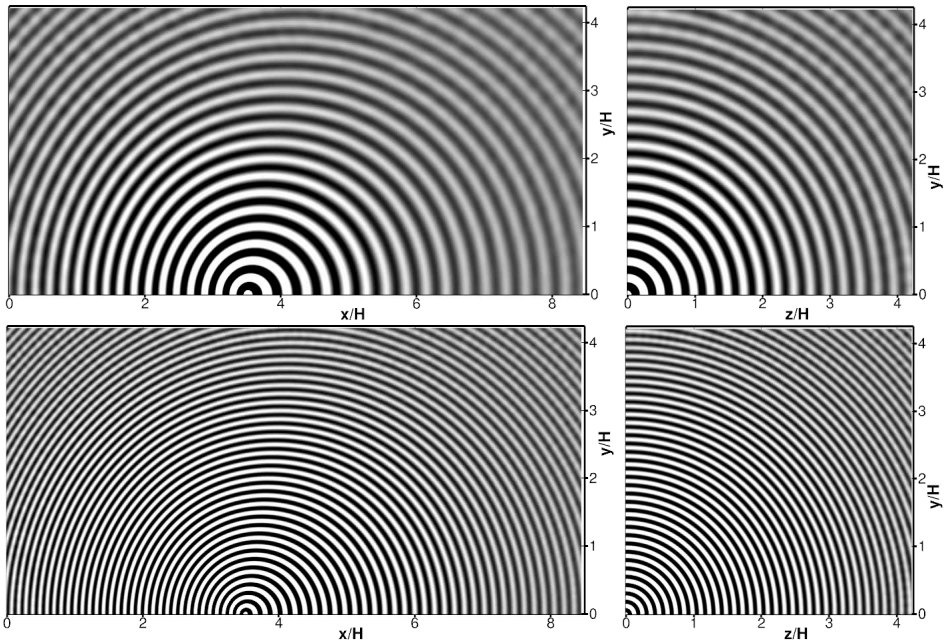

Figure 12. Numerical Assessement of Acoustic Installation Effects by QFF onto synthetic Airframe Noise Emissions, via *CAA calculations based on an equivalent monopole source emitting at various frequencies (from f_1 =1.115 kHz to f_8 = 8.92 kHz) within QFF environment : calculation case #2 (free field, uniform flow). Instantaneous snapshot of the perturbed pressure field radiated by the sources of frequency f_4 (top) and f_8 (bottom). Lateral cuts along the xy (left) and yz (right) half-planes passing by the source.*

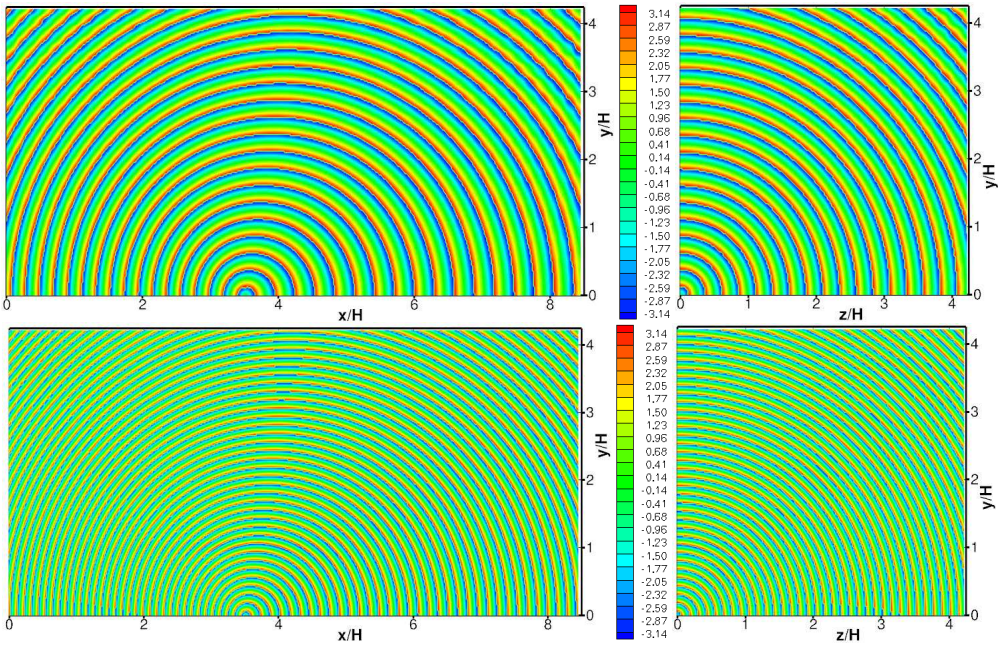

Figure 13. Numerical Assessement of Acoustic Installation Effects by QFF onto synthetic Airframe Noise Emissions, via *CAA calculations based on an equivalent monopole source emitting at various frequencies (from f_1 =1.115 kHz to f_8 = 8.92 kHz) within QFF environment : calculation case #2 (free field, uniform flow). Iso-phase fronts (φ = 0) map of the perturbed pressure field radiated by sources of frequency f_4 (top) and f_8 (bottom). Lateral cuts along the xy (left) and yz (right) half-planes passing by the source.*

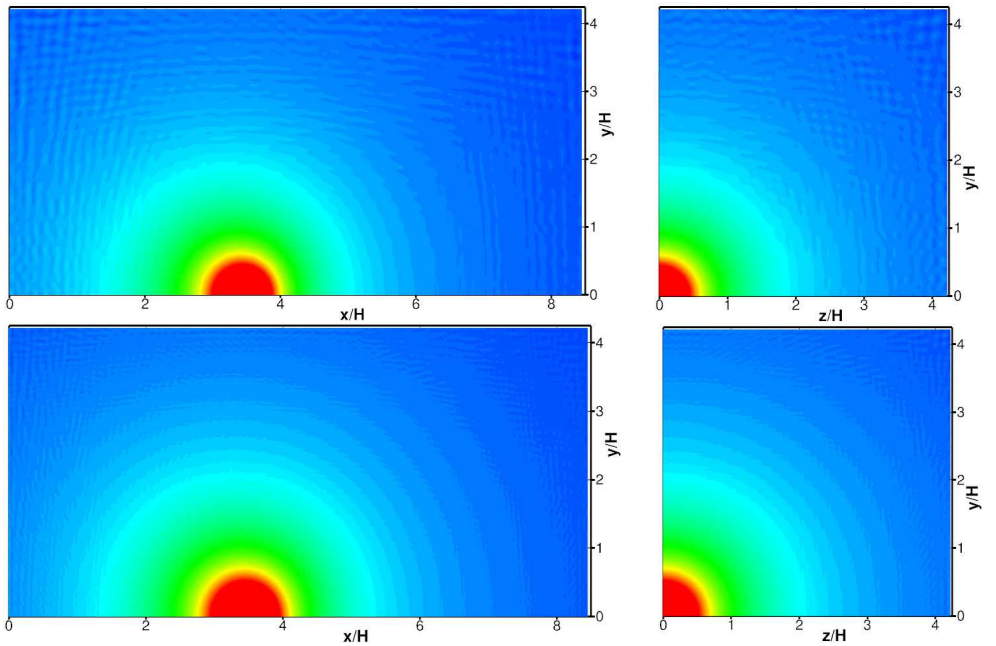

Figure 14. Numerical Assessement of Acoustic Installation Effects by QFF onto synthetic Airframe Noise Emissions, via *CAA calculations based on an equivalent monopole source emitting at various frequencies (from f_1 =1.115 kHz to f_8 = 8.92 kHz) within QFF environment: calculation case #2 (free field, uniform flow). RMS map of the perturbed pressure field radiated by sources of frequency f_4 (top) and f_8 (bottom). Lateral cuts along the xy (left) and yz (right) half-planes passing by the source.*

More important, this second calculation was taken as a reference solution for highlighting the cumulated effects by the QFF environment onto the various sources. To illustrate this point, and still regarding the 4th (resp. 8th) tones, Fig. 15 (resp. 16) displays the difference between the RMS maps of perturbed pressure fields delivered by the QFF-installed jet (calculation #1) and the free-field medium / uniform flow (calculation #2) cases. As one can see, except nearby the source location where they obviously match better, both results differ

considerably. In particular, the acoustic reinforcement / cancellation effects previously seen in Fig. 10 emerge here more clearly; those effects are non negligible at all angles, especially at the vertical of the test section (i.e. in the fly-over direction, where near- and far-field microphones are located).

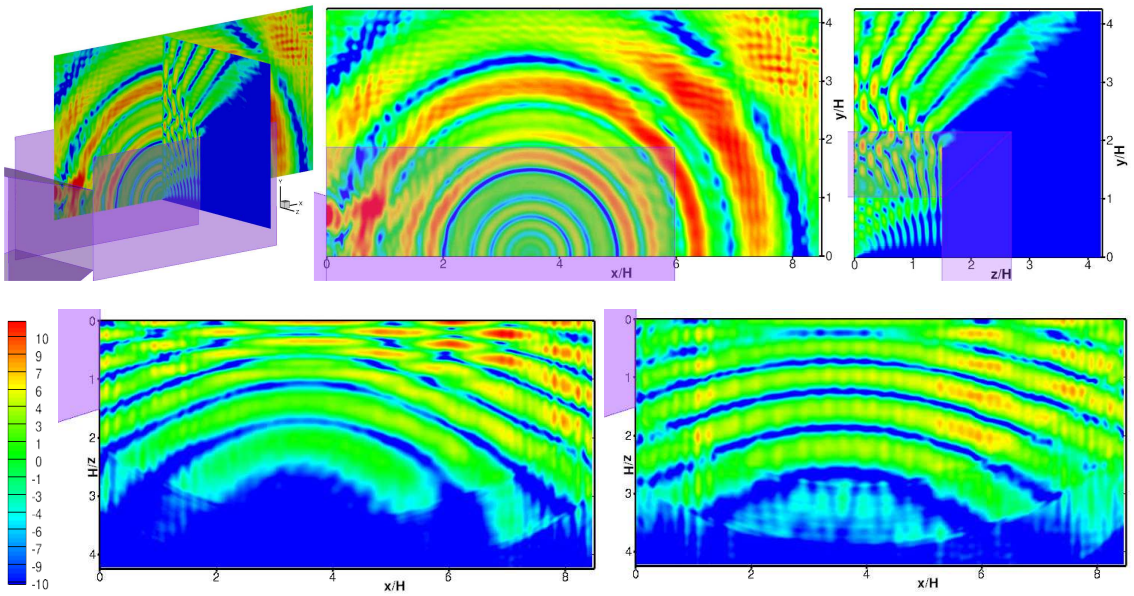

Figure 15. Numerical Assessement of Acoustic Installation Effects by QFF onto synthetic Airframe Noise Emissions, via *CAA calculations based on an equivalent monopole source emitting at various frequencies (from f_1 =1.115 kHz to f_8 = 8.92 kHz) within QFF environment: calculation cases #1 (side plates, jet flow) vs. #2 (free field, uniform flow). Delta (in dB) between the RMS maps of the perturbed pressure field radiated by source of frequency f_4 within either QFF environment (side plates, jet flow) or a homogenous medium (free-field, uniform flow). Top: 3D view (left) and lateral cuts along either the xy (center) or the yz (right) half-planes passing by the source. Bottom: lateral cuts along two xz half-planes located above the test section (left: y = 3H, right: y =4H)*

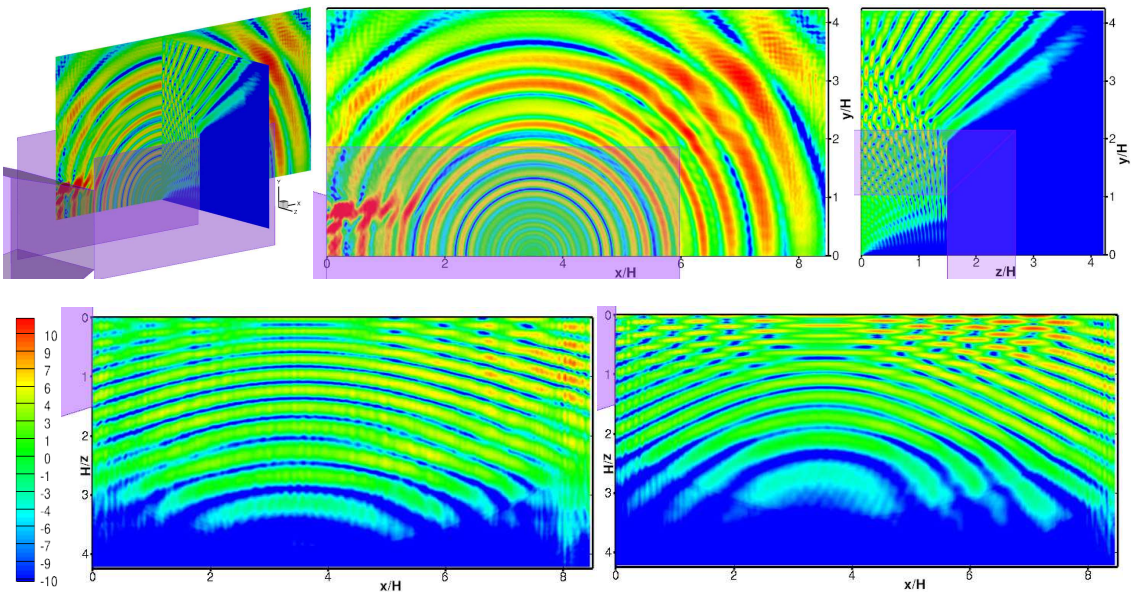

Figure 16. Numerical Assessement of Acoustic Installation Effects by QFF onto synthetic Airframe Noise Emissions, via *CAA calculations based on an equivalent monopole source emitting at various frequencies (from f_1 =1.115 kHz to f_8 = 8.92 kHz) within QFF environment: calculation cases #1 (side plates, jet flow) vs. #2 (free field, uniform flow). Delta (in dB) between the RMS maps of the perturbed pressure field radiated by source of frequency f_8 within either the QFF environment (side plates, jet flow) or a homogenous medium (free-field, uniform flow). Top: 3D view (left) and lateral cuts along either the xy (center) or the yz (right) half-planes passing by the source. Bottom: lateral cuts along two xz half-planes located above the test section (left: y = 3H, right: y =4H)*

Indeed, as one can see, the RMS deltas between the two configurations can easily exceed 10 dB in that direction. As an illustration, for each figure, the two bottom images depict the deltas in RMS levels recorded along two *xz* half-planes that are located above the test section (at a distance of 3*H* and 4*H* from the jet axis, respectively). As one can see, these deltas are non negligible (with values that oscillate between 6 and 10 *dB* over a relatively large area), exhibiting more proeminent levels downstream the source location. From what precedes, one can expect the MADA acquisition system (which crosses these two particular *xz* planes in their downstream parts) to be exposed to a non negligible amount of the acoustic installation effects highlighted here.

As was said, these installation effects result from the cumulative i) reflection/diffraction by the side plates and ii) convection/diffraction by the jet flow. With the view of isolating the sole diffraction effect by the shear layers of the present QFF-installed jet, finally, a third calculation was performed; for such calculation case #3, the side plates where kept (i.e. as in calculation case #1), but the mean flow was taken as uniform, corresponding exactly to the one used for calculation case #2. In other words, the configuration incorporated all installation effects previously highlighted, to the exception of the diffraction by the QFF jet shear layers.

Regarding such a 'side plates / uniform flow' calculation case #3, Figures 17, 18 and 19 respectively display the instantaneous, the RMS and the iso-phase fronts maps associated with the perturbed pressure field radiated by either the 4th or the 8th tonal source. As these three figures show, acoustic radiation patterns match quite closely the ones previously obtained for the 'side plates / jet flow' calculation case #1 (compare for instance the present results with those provided in bottom images of Fig. 9-a and 9-b, in Fig. 10 and in Fig. 11). From that observation, on can infer that, here again, the effects by the QFF jet flow are rather modest in regard to those induced by the side plates.

A closer look to the results indicates however that, although not proeminent, these refraction effects by the QFF-installed jet flow are not totally negligible. In particular, by comparing results depicted in Fig. 18 (resp. 19) to the ones provided in Fig. 10 (resp. 11), it appears that the acoustic levels reinforcements one could previously observe along that part of the shear layer which is located upstream the source (see Fig. 15 & 16) are no longer present. This confirms that they were effectively due to the refraction by the shear layers of such QFF jet flow. From a more global point of view, by comparing the maps of iso-phase fronts associated with these two calculation cases #1 and #3 (compare for instance results of Fig. 11 to the ones of Fig. 19), one can see how both patterns differ noticeably all over the domain, translating how acoustic waves are phase-shifted as they cross the jet shear layers. Here it is worth mentioning that the acoustic measurements usually performed via the far-field microphones are much sensitive to an alteration of the acoustic amplitude than to a modification of its phase pattern. Such tendency, however, is inverted when it comes to apply experimental techniques of source localization (such as is done via MADA acquisition system), for which an accurate identification of acoustic phases is critical. This underlines the crude necessity of characterizing at best this alteration of acoustic phase fronts due to refraction effects by the QFF jet.

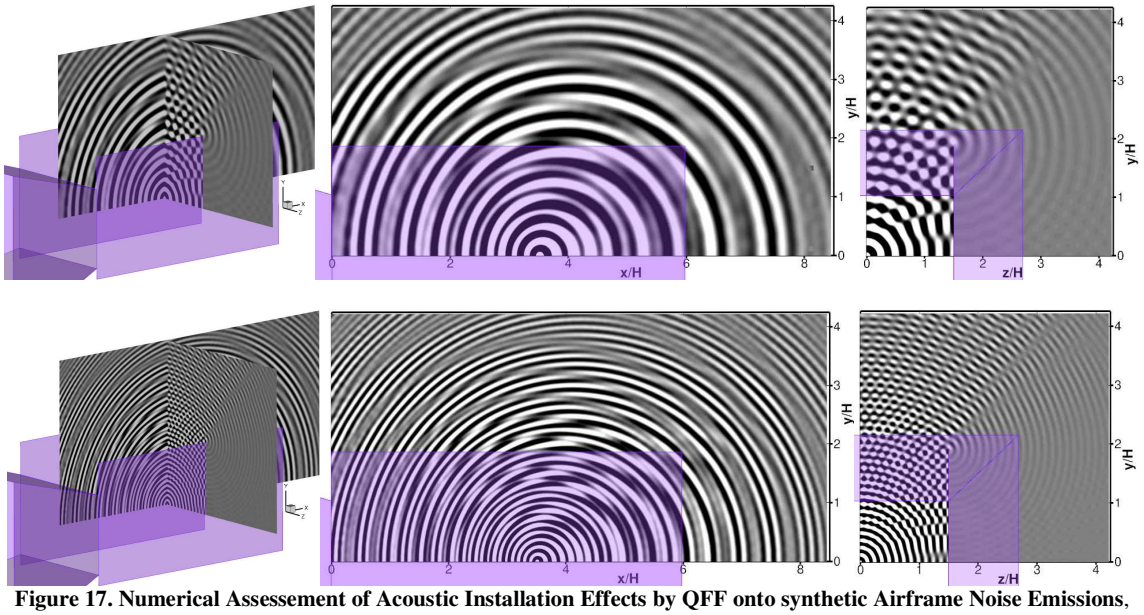

Figure 17. Numerical Assessement of Acoustic Installation Effects by QFF onto synthetic Airframe Noise Emissions, via *CAA calculations based on an equivalent monopole source emitting at various frequencies (from f_1 =1.115 kHz to f_8 = 8.92 kHz) within QFF environment : calculation case #3 (side plates, uniform flow). Instantaneous snapshot of the perturbed pressure field radiated by sources of frequency f_4 (top) and f_8 (bottom). 3D views (left), and lateral cuts along the xy (center) and yz (right) half-planes passing by the source. QFF nozzle is here drawn for indicative purpose only.*

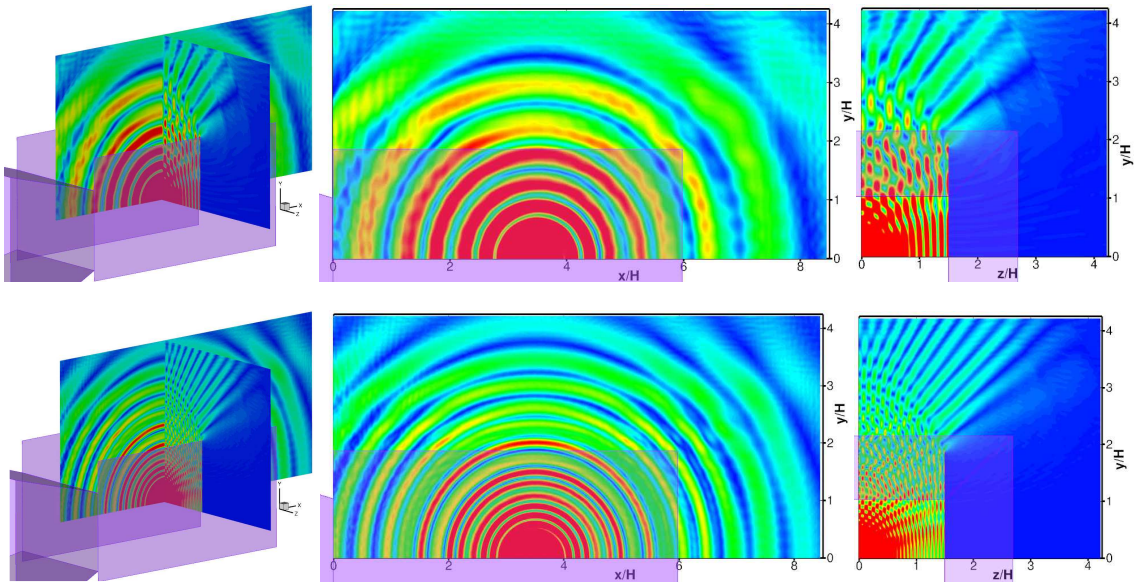

Figure 18. Numerical Assessement of Acoustic Installation Effects by QFF onto synthetic Airframe Noise Emissions, via *CAA calculations based on an equivalent monopole source emitting at various frequencies (from f_1 =1.115 kHz to f_8 = 8.92 kHz) within QFF environment: calculation case #3 (side plates, uniform flow). RMS map of the perturbed pressure field radiated by sources of frequency f_4 (top) and f_8 (bottom). 3D views (left), and lateral cuts along the xy (center) and yz (right) half-planes passing by the source. QFF nozzle is here drawn for indicative purpose only.*

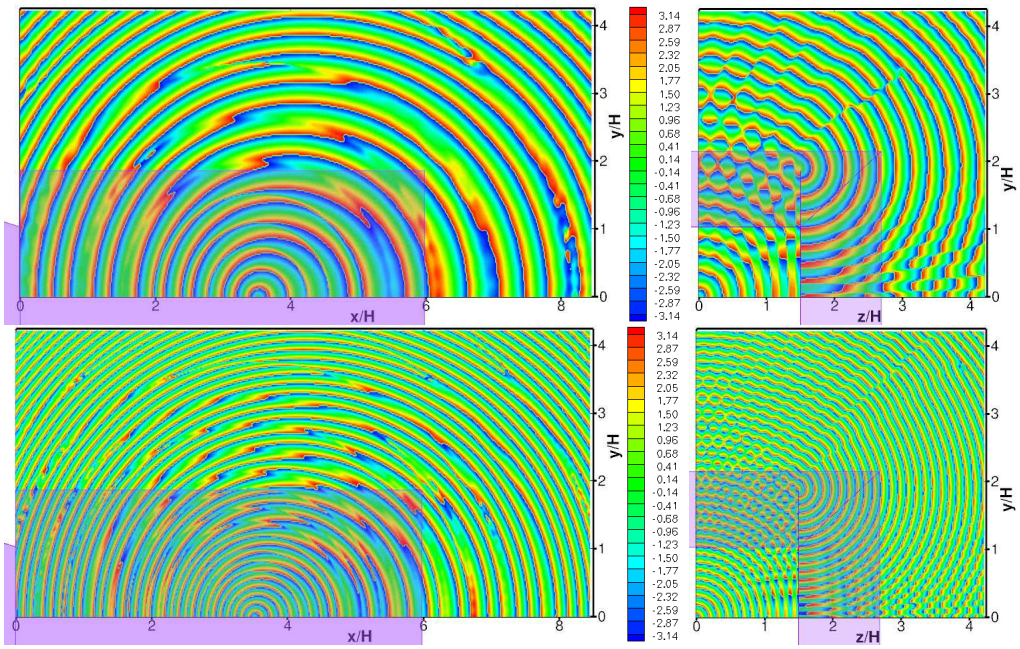

Figure 19. Numerical Assessement of Acoustic Installation Effects by QFF onto synthetic Airframe Noise Emissions, via *CAA calculations based on an equivalent monopole source emitting at various frequencies (from f_1 =1.115 kHz to f_8 = 8.92 kHz) within QFF environment: calculation case #3 (side plates, uniform flow). Iso-phase fronts (φ = 0) map of the perturbed pressure field radiated by sources of frequency f_4 (top) and f_8 (bottom). 3D views (left), and lateral cuts along the xy (center) and yz (right) half-planes passing by the source. QFF nozzle is here drawn for indicative purpose only.*

On this stage, one can notice that all the observations previously made about refraction effects by QFF jet flow (amplitude reinforcements, phase shifting, etc.) are coherent with what can be observed in reality, and - to some extent - predicted by the theory (e.g. works by Amiet[16]). This is why follow-on computations[22] are planned, which objective will be to check the validity of the infinitely thin shear layer assumption of Amiet's corrections[16] (that are commonly applied to QFF experimental data). One can here recall that the latter

corrections are based on an *isolated* jet, of either an axisymmetric (round jet) or a two-dimensional (shear layer) nature. Therefore, these alternative computations will not incorporate any of the QFF set-up devices, the propagation medium being defined as a free-field, as in calculation case #2. In contrast to the latter case, however, the mean flow will be allotted a two-dimensional shear layer, of either infinitely thin or thick nature. These alternative CAA calculations will be compared with results coming from the ray tracing technique proposed by Candel in the 70's. This shall provide a unique opportunity to compare CAA and ray tracing approaches, in regard to their respective abilities to assess installation effects characterizing realistic facility environments. From a more methodological point of view, the outcomes of this prospective study[22] should help further assess acoustic installation effects that may be important in the type of testing typically done in the NASA/LARC QFF facility.

V. Conclusions

The present study focused on the acoustic installation effects that may occur in the NASA Langley Research Center anechoic facility named QFF (Quiet Flow Facility). CAA calculations based on equivalent simplistic sources were performed, allowing a numerically evaluation of the acoustic installation effects induced by the various components (e.g., mounting side plates, nozzle, collector plate) or features (e.g., confined jet vs. co-flow) characterizing the NASA/LaRC QFF facility.

First, a low frequency dipole noise source was considered, so as to model the noise emission observed in the so-called Tandem Cylinder (TC) experiments that had been originally achieved at QFF. Results both confirmed and expanded upon the conclusions that had been previously made in an earlier assessment of QFF installation effects on the TC experiment, which had been achieved using a CFD-CAA hybrid approach. Then, additional simulations employed other equivalent sources along with different QFF operating conditions, so as to generalize these particular conclusions to the airframe noise tests that are more typically conducted within the QFF.

At the light of these studies, it appears that it is less the refraction effects by the jet flow than the reflection / diffraction effects by the set up devices that have the largest effect on the acoustic signature of models to be tested in QFF. One should emphasize that such effects may act very differently on the various source components, depending on their respective frequency. On another hand, and although they appear to be rather modest in regard to those induced by the apparatus, the refraction effects by the QFF jet flow impact the noise propagation in a non-negligible way, especially for what concerns the acoustic phase.

Follow-on computations are planned to provide a more complete numerical assessment of such diffraction effects associated with the spreading of the QFF jet. In particular, additional jet flows will be considered (infinitely thin or thick shear layer, etc.), so as to check the validity of the infinitely thin shear layer correction that is commonly applied to QFF experimental data. The outcome of this prospective study should help further assess acoustic installation effects that may be important in the type of testing typically done in the NASA/LARC QFF facility.

Acknowledgments

The present study was achieved as part of the International Agreement between NASA and Onera on "*Understanding and Predicting the Source of Nose Landing Gear Noise*". The author greatly acknowledges Dr. David Lockard, Dr. Mehdi Khorrami and Dr. Meelan Choudhari (all from NASA/LaRC) for their continuous support, help and guidance in the definition and achievement of this work. The author also thanks other NASA/LaRC personnel, such as Dr. Florence Hutcheson and Mr. Daniel Stead for the detailed information regarding the QFF experimental set up, as well as Dr. Ana Tinetti whose past works motivated the present study. Finally, the author is grateful to Dr. J. Bulte (from Onera) for the key insights he provided him with, regarding physics and theoretical modeling of refraction effects by sheared flows.

References

[1]Jenkins, L. N., Khorrami, M. R., Choudhari, M. M. and McGinley, C. B., "Characterization of Unsteady Flow Structures Around Tandem Cylinders for Component Interaction Studies in Airframe Noise," AIAA Paper *2005-2812*, 11th AIAA/CEAS Aeroacoustics Conference, Monterey, USA, May 23-25, 2005.

[2]Hutcheson, F. V. and Brooks, T. F., "Noise Radiation from Single and Multiple Rod Configurations," AIAA Paper *2006-2629*, 12th AIAA/CEAS Aeroacoustics Conference, Cambridge, USA, May 2006.

[3]Lockard, D. P., Khorrami, M. R., Choudhari, M. M., Hutcheson, F. V. and Brooks, T. F., "Tandem Cylinder Noise Prediction," AIAA Paper *2007-3450*, 13th AIAA/CEAS Aeroacoustics Conference, Roma, Italy, May 2007.

[4]Kirchhoff, G. R., "Zur Theorie der Lichtstrahlen," *Annalen der Physik und Chemie*, Vol. 18, 1883, pp. 663–695.

[5]Lighthill, M.J., "On Sound Generated Aerodynamically. I. General theory / II. Turbulence as a source of sound," *Proc. Roy. Soc. London*, Vol. **A 211**, 1952 / Vol. **A 222**, 1954.

[6]Ffowcs-Williams, J. E. and Hawkings, D. L., "Sound Generation by Turbulence and Surfaces in Arbitrary Motion," *Philosophical Transactions of the Royal Society of London* A, Vol. **342**, 1969, pp. 264–321.

[7]Redonnet, S., "Aircraft Noise Prediction via AeroAcoustics Hybrid Methods: A Decade of Development and Application of Onera Tools," to appear in *Aerospace Lab Journal* (2014).

[8]Redonnet, S., Manoha, E. and Sagaut, P. "Numerical Simulation of Propagation of Small Perturbations interacting with Flows and Solid Bodies," *AIAA Paper n° 2001-2223*, 7th CEAS/AIAA Aeroacoustics Conference, Maastricht, The Netherlands, May 2001.

[9]Redonnet, S., "Simulation de la propagation acoustique en présence d'écoulements quelconques et de structures solides, par résolution numérique des équations d'Euler," *PhD Thesis*, Université Bordeaux I, December 2001.

[10]Redonnet, S., Desquesnes, G., Manoha, E. and Parzani, C., "Numerical Study of Acoustic Installation Effects with a CAA Method," *AIAA Journal*, Vol 48 n°5, May 2010.

[11]Redonnet, S. and Druon, Y., "Computational AeroAcoustics of Realistic Co-Axial Engines," *AIAA Journal*, Vol 50 n°5, May 2012.

[12]Redonnet, S., Lockard, D. P., Khorrami, M. R. and Choudhari, M. M., "CFD-CAA Coupled Calculations of a Tandem Cylinder Configuration to Assess Facility Installation Effects," *AIAA Paper 2011-2841*, 17th AIAA/CEAS Aeroacoustics Conference, Portland, USA, June 2011.

[13]Redonnet, S., "On the Numerical Prediction of Aerodynamic Noise via a Hybrid Approach - Part 1: CFD/CAA Surfacic Coupling Methodology, Revisited for the Prediction of Installed Airframe Noise Problem*," AIAA Paper 2010-3709*, 16th AIAA/CEAS Aeroacoustics Conference, Stockholm, Sweden, June 2010.

[14]Redonnet, S., "The Non Reflective Interface: An Innovative Forcing Technique for Computational Acoustic Hybrid Methods," to be submitted for publication in *International Journal for Numerical Methods in Fluids* (2014).

[15]Tinetti, A. F. and Dunn, M. H. , "Acoustic Simulations of an Installed Tandem Cylinder Configuration," AIAA Paper n°2009-3158, 15th AIAA/CEAS AeroAcoustics Conference, Miami, USA, May 2009.

[16]Amiet R. K., "Correction of open jet wind tunnel measurements for shear layer refraction," *AIAA paper 75-532*, 2nd AIAA Aeroacoustics Conference, Hampton, 1975.

[17] Cunha, G. and Redonnet, S., "Low-Dispersion High-Order Explicit Finite-Difference Schemes for Computational Aeroacoustics," submitted for publication in *International Journal for Numerical Methods in Fluids*, October 2013.

[18]S. K. Lele, "Compact finite difference schemes with spectral-like resolution," *Journal of Computational Physics* **103** (1) (1992) 16–42.

[19]C. K. W. Tam, J. C. Webb, "Dispersion-relation-preserving finite difference schemes for computational acoustics," *Journal of Computational Physics* **107** (8) (1993) 262–281.

[20]Redonnet, S., Cunha, G., and Ben Khelil, S., "Numerical Simulation of Landing Gear Noise via Weakly Coupled CFD-CAA Calculations," AIAA paper 2013-2068, 19th AIAA/CEAS Aeroacoustics Conference, Germany, June 2013.

[21]Humphreys W. M. and Brooks T. F., "Noise Spectra and Directivity for a Scale-Model Landing Gear," AIAA paper 2007-3458, 13th AIAA/CEAS Aeroacoustics Conference, Italy, May 2007.

[22]Redonnet, S., and Bulte, J., "Computational and Theoretical Investigation of the Refraction Effects by Jet Flows in Anechoic Wind Tunnels", to be presented at the 43rd International Congress and Exposition on Noise Control Engineering (Internoise 2014 Conference), Australia, October 2014.